

AEROACOUSTICS OF BLADE VORTEX INTERACTION USING INDICIAL AERODYNAMICS AND THE ACOUSTIC ANALOGY

J. Gordon Leishman*

Center for Rotorcraft Education and Research

Department of Aerospace Engineering

Glenn L. Martin Institute of Technology

University of Maryland at College Park

Abstract

The aeroacoustics of blade vortex interaction (BVI) has been investigated using indicial aerodynamics combined with the acoustic analogy in the form of the Ffowcs Williams-Hawkins (FW-H) equation. Generalized subsonic indicial lift functions for the lift on an airfoil penetrating a stationary sharp-edge gust were used as a basis for the unsteady airloads. Alternative indicial gust functions were derived from subsonic linear theory and from a direct numerical simulation of the indicial gust problem using computational fluid dynamics (CFD). For the 2-D airfoil-vortex interaction problem at various free-stream Mach numbers the indicial method was compared with CFD results with good agreement below the critical Mach number. The indicial method was integrated into a three-dimensional simulation of an idealized BVI problem in a manner that would be used in a comprehensive rotor analysis. Good agreement was found with simultaneously measured airloads and acoustics.

Nomenclature

a	Sonic velocity, ms^{-1}
c	Blade chord, m
c_{ref}	Reference chord, m
C_n^g	Normal force coefficient due to gust
ΔC_p	Differential pressure coefficient
E	Complete elliptic integral of 2nd kind
$E'(\Psi)$	Incomplete elliptic integral of 2nd kind
$F'(\Psi)$	Incomplete elliptic integral of 1st kind
G_i	Coefficients of sharp-edged gust function
g_i	Exponents of sharp-edged gust function
k	Modulus of elliptic integrals
k_g	Gust reduced frequency
K	Complete elliptic integral of 1st kind
$l_{\mathcal{R}}$	Force on fluid in direction of \mathcal{R} , N
M	Local free-stream Mach number
$M_{\mathcal{R}}$	Relative Mach number between source and receiving point
p'	Fluctuating pressure, Pa
r	Radial distance from vortex center, m
r_c	Vortex core radius, m
R	Rotor radius, m
\mathcal{R}	Distance from source to observer, m
s	Distance in semi-chords = $2Vt/c$
S	Blade area, m^2

t	Time, s
v_n	Normal perturbation velocity, ms^{-1}
V	Velocity, ms^{-1}
V_θ	Tangential velocity, ms^{-1}
V_T	Local (blade-element) velocity, ms^{-1}
V_g	Gust convection velocity, ms^{-1}
V_∞	Free-stream velocity, ms^{-1}
w_g	Gust velocity normal to airfoil, ms^{-1}
x, y	Airfoil coordinate system, measured from leading edge, m
x'	Dummy variable of integration, m
x_v, y_v, z_v	Position of vortex, m
y_t	Airfoil thickness envelope, m
Z_i	Aerodynamic deficiency functions
α	Angle of attack, $rad.$
α_e	Effective angle of attack, $rad.$
β	Glauert factor = $\sqrt{1 - M^2}$
Γ	Vortex strength (circulation), m^2/s
$\hat{\Gamma}$	Non-dimensional strength = $\Gamma/V_\infty c_{ref}$
Δ	Incremental quantity
λ	Gust speed ratio, = $V/(V + V_g)$
ρ	Air density, $kg\ m^{-3}$
τ	Retarded time, s
ϕ	Indicial response function
ψ_b	Blade azimuth
ψ_g	Sharp-edged gust function
ψ	Rotor azimuth, $deg.$
ψ_τ	Retarded azimuth, $deg.$
Ψ	Argument of elliptic integrals
Ω	Rotor frequency, $rad./s$
σ	Dummy variable of integration

Introduction

The rotor blades of helicopters and tilt-rotor aircraft can encounter large velocities and intense velocity gradients that are generated by tip vortices trailed from previous blades. These blade vortex interactions (BVI) produce significant unsteady effects that become particularly acute when the axis of the tip vortex is parallel, or almost parallel, to the leading-edge of the blade. This occurs primarily on the advancing and retreating sides of the rotor disk during low speed descents or during maneuvering flight. BVI has been identified not only as a significant source of unsteady aerodynamic loading, but also a major contributor to rotor noise.¹⁻³ The obtrusive and highly focused nature of BVI noise means that accurate predictions of the phenomenon are becoming essential aspects of the rotor design process. This is essential to alleviate landing approach noise levels in civilian rotorcraft op-

*Associate Professor.

Presented at the 22nd European Rotorcraft Forum, 17-19 September 1996, Brighton, UK. Copyright ©1996 by the Royal Aeronautical Society. All rights reserved.

erations, and to help reduce aircraft detectability in military applications.

Many experimental and numerical research studies have provided a good amount of fundamental knowledge about the BVI phenomenon. This has led to an increased appreciation of the complex physical nature of the flow and the difficulties in prediction.⁴⁻⁸ Pure CFD approaches to rotor far-field BVI acoustics are not yet practical because of numerical dissipation. Also, while coupled CFD and Kirchhoff based methods have provided significant insight into aeroacoustic phenomena, they are still far too computationally expensive for rapid parametric studies.^{9, 10} Bearing in mind that accurate predictions of BVI will involve blade structural dynamic and aerodynamic modeling as a fully integrated system including sophisticated free-wake modeling, this places serious constraints on the allowable levels of unsteady aerodynamic modeling. In addition, with the increasing trend toward the development of active rotor control technologies such as blade mounted trailing-edge flaps,¹¹⁻¹³ there is a need for improved unsteady aerodynamic models that also need to be in specific mathematical forms so they can be used for studies in active acoustic control.

While a good model for the unsteady aerodynamics is the key to the acoustic problem, in the interests of computational brevity most comprehensive rotor models contain much less sophisticated unsteady aerodynamic models compared to those actually required. The BVI phenomenon is often referred to as a "leading-edge problem," but the leading-edge pressure response is dominant for all situations involving changes in blade section angle of attack. The important issues for modeling the acoustics are to represent the effects of compressibility and unsteady (time-history) effects on the sectional (leading-edge) pressure loading. Even when the sectional aerodynamics model may include some level of unsteady modeling, the approaches used in many rotor codes do not properly distinguish the aerodynamic effects at the blade element level due to the wake induced velocity from the aerodynamics due to changes in angle of attack and pitch rate. The former can be considered as a convecting gust field through which the blade section penetrates, while the latter will be due to blade motion such as flapping, cyclic pitch control inputs for trim, and blade torsional response. Each produces a different source of unsteady aerodynamic loading and time-history. Therefore, not only is the lack of distinction between gust encounters and changes in angle of attack or pitch rate fundamentally incorrect, but it may lead to erroneous predictions of the unsteady airloads and resulting acoustics. The significant predictive deficiencies compared to experiment and the large code-to-code variability of the acoustic results shown in Ref. 14 suggests that significant fundamental work still remains to be done.

The present work focuses on the use of an indicial aerodynamic model to calculate the unsteady aerodynamics due to the rotor wake and BVI. A good review of the general indicial concept is given by Lomax¹⁵ and Tobak and Schiff.¹⁶ If the indicial response can be found, then the unsteady aerodynamic response to an arbitrary input (forcing) can be found by Duhamel superposition. The indicial response in some cases is known analytically,¹⁷⁻²⁰ in other cases

numerically,^{20, 21} and it can also be found experimentally by inverse techniques using the aerodynamic response to sinusoidal forcing.²²⁻²⁴ If the linearity of the flow physics over the required range of conditions can be justified, then one advantage of the indicial method is a tremendous saving in computational cost over performing separate flow field calculations. By using certain analytic forms of the indicial response, the unsteady aerodynamic model can be written in a numerical form suitable for implementation in comprehensive rotor aeroacoustic model, and also in a form that can be utilized by a control algorithm.

The methodology in the present article is developed in a form used previously for unsteady airfoil motion^{25, 26}, unsteady flap motion²⁷⁻²⁹ and dynamic stall.³⁰⁻³³ Therefore, the algorithms can be easily appended to those already in use. The results indicate that good economical predictions of the unsteady airloads for problems such as BVI are possible using the indicial method. When the predictions of the unsteady airloads are coupled to the FW-H equation, the results also show good agreement with measured near-field and far-field acoustics generated by BVI.

Methodology

BVI can be considered as a transient gust problem. Incompressible time-dependent solutions for gust problems on 2-D airfoils have been obtained by Küssner,¹⁸ Von Karman and Sears,¹⁹ Horlock³⁴ and Miles.³⁵ For the general vertical gust problem in incompressible flow, Duhamel superposition can be used with the Küssner sharp-edge gust function, $\psi_g(s)$, to find the aerodynamic loads due to an arbitrary stationary gust field. The equivalent sharp-edge gust solutions for the subsonic case can be obtained only approximately,^{15, 20} but even then the functions are not easily represented in a mathematical form suitable for practical calculations.

For the traveling vertical gust case, which is the most general situation, the problem was solved for incompressible flow by Miles³⁵ in terms of the gust parameter $\lambda = V/(V + V_g)$. As the propagation speed of the traveling gust increases from zero to ∞ (λ decreases from 1 to 0), the solution changes from the Küssner result to the Wagner result,³⁶ with a variety of intermediate transitional results being obtained. However, in the rotor environment, the convected wake velocities are generally much lower than the local blade element velocity, so the assumption that $\lambda \approx 1$ is usually valid, and the stationary sharp-edge gust result can be assumed. This produces a justifiable level of simplification in the unsteady aerodynamic modeling that retains the efficiency necessary for a comprehensive rotor aeroacoustics simulation.

Note that in linear theory only the vertical component of the gust is used to satisfy the boundary conditions; unsteady effects due to the in-plane component of the gust velocity can usually be ignored since it is known that horizontal disturbances produce only a quasi-steady effect to a first-order.^{6, 34, 37} See also Goldstein³⁸ for a discussion of this point. However, unsteady in-plane effects may be a more significant factor affecting the airloads if the blade passes into the high rotational velocities in the core of a vortex, especially under transonic conditions. However, the

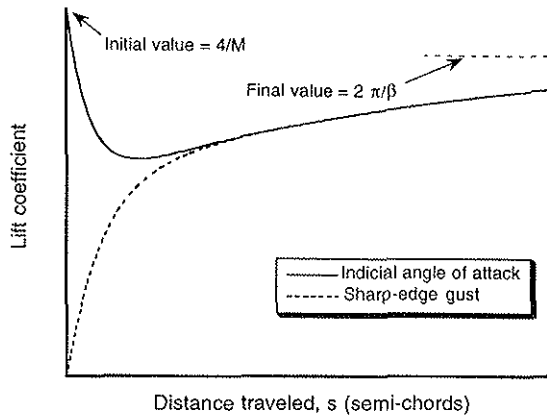


Figure 1: Comparison of indicial lift response due to a step change in angle of attack and the penetration of a stationary sharp-edge gust

bounds of linearity in such cases can probably be only understood with the use of CFD methods.

2-D Exact Subsonic Linear Theory

In the indicial angle of attack case, the boundary conditions change instantaneously over the chord. This produces a finite (noncirculatory) value at $s = 0$, as given by linear piston theory,³⁶ followed by a rapid decay because of the propagation of wave disturbances at the speed of sound. This is then followed by a gradual and asymptotic growth in lift because of the growth in circulation about the airfoil – see Fig. 1. By convention, s represents the distance traveled by the airfoil in semi-chords. The physics during this transient process are rather complicated because of the propagation of downstream and upstream moving wave fronts (non-circulatory effects), combined with the simultaneous creation of circulation. In the case of a sharp-edge gust, the boundary conditions change progressively across the chord, so the lift is zero at the initiation of gust penetration but builds rapidly and approaches the angle of attack result at later times. Again, the physics during this transitional process are rather complicated, and even with linearity assumptions there are no equivalent exact solutions to the Küssner function for the subsonic flow case.

The sharp-edge gust problem in subsonic flow was examined by Lomax³⁹ using the method of supersonic analogy. The actual calculations are fairly elaborate, but exact analytical expressions for the airfoil pressure distribution can be found for a limited period of time after the gust entry. For the period $0 \leq s \leq 2M/(1+M)$ (which corresponds to less than 1-chord length of travel even at $M = 0.7$) the airfoil pressure distribution for a unit gust disturbance is given exactly by

$$\Delta C_p(x, \hat{t}) = \frac{8}{\pi(1+M)} \sqrt{\frac{M(\hat{t}-x)}{x+M\hat{t}}} \quad (1)$$

where x is measured from the airfoil leading-edge and $\hat{t} = at$. When this equation is integrated, the result

for the unsteady normal force for a unit gust is

$$\Delta C_n^g(s) = \frac{2s}{\sqrt{M}} \quad (2)$$

For later values of time up to $s = 4M/(1-M^2)$, solutions for the airfoil pressure distribution during the gust penetration are also known exactly³⁹ but take on a much more complicated form. Again, for a unit gust

$$\begin{aligned} \Delta C_p(x, \hat{t}) = & \frac{8}{\pi(1+M)} \left\{ \sqrt{\frac{M(\hat{t}-x)}{x+M\hat{t}}} \right. \\ & + \frac{2}{\pi} \sqrt{M(\hat{t}-x)(c-x-M\hat{t})} \\ & \left. \left[\frac{2K}{\sqrt{(\hat{t}^2-x^2)(1-M^2)}} \right. \right. \\ & \left. \left. + \frac{EF'(\Psi) + KE'(\Psi) - KF'(\Psi)}{\sqrt{(x+M\hat{t})(c-x-M\hat{t})}} \right] \right\} \quad (3) \end{aligned}$$

where E , K , $E'(\Psi)$ and $F'(\Psi)$ are elliptic integrals of various kinds with modulus k given by

$$k = \sqrt{\frac{(\hat{t}+x)(1+M) - 2c}{(\hat{t}+x)(1+M)}} \quad (4)$$

and argument $\Psi = \sin^{-1} \sqrt{(x+M\hat{t})/c}$. These equations can only be integrated numerically.

Interestingly, the pitching moment during the gust penetration is found to asymptote to the 1/4-chord in the short time $s = 2M/(1+M)$, suggesting that the variation of the moment can be safely ignored. However, in a practical sense the effects of viscosity will modify the effective aerodynamic center so that some aerodynamic moment will always be produced on the airfoil as it moves through a gust field.

For $s > 4M/(1-M^2)$ there are no analytic solutions possible in the subsonic flow case and more approximate methods of finding the indicial function must be adopted, see Lomax *et al.*²⁰ and Lomax.³⁹ However, the asymptotic result for a unit gust is simply given by the conventional steady-state theory, namely

$$\Delta C_p(x, \hat{t} = \infty) = \frac{4}{\beta} \sqrt{\frac{1-x}{x}} \quad (5)$$

so that

$$\Delta C_n^g(s = \infty) = \frac{2\pi}{\beta} \quad (6)$$

For $4M/(1-M^2) \leq s < \infty$, the chordwise pressures cannot be determined analytically but one can use a relationship between the gust function ψ_g and the indicial response to a step change in angle of attack, ϕ_α , as shown by Garrick.⁴⁰ Unfortunately, in the subsonic case no exact solutions are possible for either ϕ_α or ψ_g . However, indicial angle of attack results have been obtained, albeit approximately, by Mazelsky^{22, 23} and Leishman.²⁴ These results can be used in some cases to complete the indicial gust responses by numerical approximation at later values of time.

Direct Indicial Simulation by CFD

CFD solutions can provide results for many practical problems that cannot be solved analytically or simulated by experimentation. Yet, these solutions are only available at significant computational cost, and even then are still subject to certain approximations and limitations. Nevertheless, CFD solutions can help fill in gaps in solutions that are not available using the exact linear theory, such as for $s > 4M/(1 - M^2)$ in the above case. The non-linear physics modeled by CFD also provides additional guidance in establishing the limits of the classic linear theory, especially for airfoils with finite thickness and camber, and also when operating close to and beyond the critical Mach number.

Indicial type calculations using CFD require special treatment to avoid artificial numerical transients, and so appear relatively rarely in the published literature. However, some nonlinear indicial and gust solutions have previously been performed by and McCroskey,⁶ Stahara and Spreiter,⁴¹ and also Ballhaus and Goorjian,⁴² using various small-disturbance, full-potential, and Euler solvers. More recent indicial calculations have been performed by Parameswaran⁴³ and Singh⁴⁴ who have computed airloads for indicial angle of attack, pitch rate and sharp-edged gusts using the TURNS (Transonic Unsteady Rotor Navier-Stokes) code.⁴⁵ These latter results, which consider both 2-D and 3-D indicial problems, are extremely useful since they help establish the bounds of linear theory and also provide good check cases for the indicial method over a range of flow conditions where exact analytical solutions are unavailable.

CFD results computed by Parameswaran⁴³ for the sharp-edged gust problem are shown in Fig. 2 for Mach numbers of 0.3 and 0.5, and are compared to the exact linear theory obtained from Eq. 2 and the integration of Eq. 3. The comparisons at earlier values of time are excellent, and certainly lend significant credibility to the CFD results. The CFD results at later values of time are also shown in Fig. 2, where it is apparent that the growth of lift is affected by compressibility effects such that at the higher Mach numbers the airfoil must travel further through the fluid for the final flow adjustments to be completed. Note that for the transonic ($M = 0.8$) case, there is a small perturbation in the curve at $s \approx 11$. This is due to the formation development of a shock wave, which alters the rate of unsteady flow adjustments. The CFD results give final values that are very close to the linear values for a flat plate as given by the Glauert correction (see also Singh and Baeder.⁴⁴)

Functional Approximations to Gust Response

A key factor in the successful application of indicial-type methods to general problems is the functional form used for the indicial response function. Because of the asymptotic growth of the indicial functions, several authors including Lomax,²⁰ Mazelsky,²² Mazelsky and Drishler,²³ and Leishman,²⁴ have used exponential approximations. While an exponential form of the indicial response is not an exact representation of the physical behavior, in most cases involving superposition with specific types of motion such as sinusous

or other periodic forcing, it has proven sufficient when compared to experimental data. However, for some applications the exponential approximation to the indicial response may be inadequate, and caution should always be exercised.

A typical exponential approximation to the sharp-edged gust is of the form

$$\psi_g(s, M) \approx 1 - \sum_{i=1}^N G_i(M) \exp \{-g_i(M)s\} \quad (7)$$

for $s \geq 0$, where the G_i and g_i coefficients are functions of Mach number. In each case we must have $\sum_{i=1}^N G_i = 1$ and $g_i > 0$ for $i = 1 \dots N$. Therefore, the lift during the penetration of a sharp-edged gust of unit magnitude is given by

$$\Delta C_n^g(t, M) = \frac{2\pi}{\beta} \psi_g(s, M) \quad (8)$$

where the steady-state value of the lift is simply the two-dimensional flat-plate result with the Glauert correction. For practical calculations it is possible to replace the linearized value of the steady lift-curve-slope, $2\pi/\beta$, in Eq. 8 by a value measured from experiment or modeled by CFD for a particular airfoil.

Unfortunately, the exponential approximation in Eq. 7 is not necessarily in the most useful form for a helicopter rotor analysis. This is because on a rotor each blade station encounters a different local Mach number as a function of blade radial location, and during forward flight the local Mach number is also a function of blade azimuth angle. Therefore, repeated interpolation of the G_i and g_i coefficients between successive Mach numbers will be required. While simple in concept, there is a surprisingly large computational overhead associated with this process.

To avoid this overhead, it has been shown^{24, 46} that the asymptotic (circulatory dominated) part of the total lift due to a step change in angle of attack in subsonic compressible flow can be approximated by a two term exponential function with coefficients that can be scaled in terms of Mach number alone. Since for later values of time it is known that the sharp-edged gust and indicial angle of attack functions approach each other, a similar behavior can be assumed valid for the sharp-edged gust function, i.e.,

$$\psi_g(s, M) \approx 1 - \sum_{i=1}^N G_i \exp \{-g_i \beta^2 s\} \quad s \geq 0 \quad (9)$$

where $\sum_{i=1}^N G_i = 1$ as before but now the G_i 's and g_i 's are fixed and considered independent of Mach number. It has already been shown in Ref. 47 that for gusts the form of this indicial function appears acceptable up to at least the critical Mach number of the airfoil section.

Determination of $\psi_g(s, M)$ from Linear Theory

As described in Ref. 47, the evaluation of the gust function coefficients in Eq. 9 can be formulated as a least-squares optimization problem with several imposed equality and inequality constraints. These include both the initial value ($\psi_g(0, M) = 0$) and final

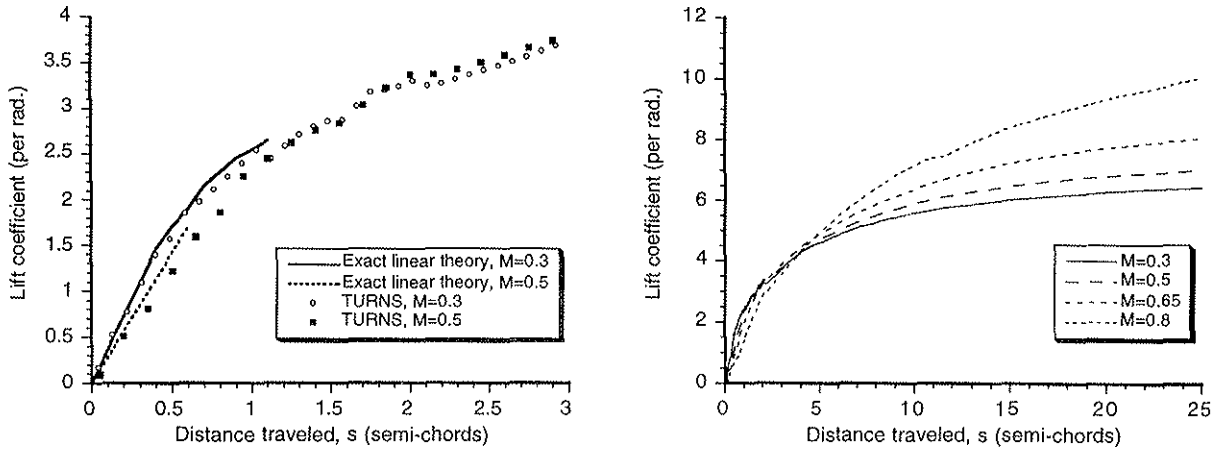


Figure 2: Unsteady lift due to the penetration of a sharp-edge gust. Left figure: Comparison of exact linear theory and TURNS. Right figure: TURNS calculations at various Mach numbers

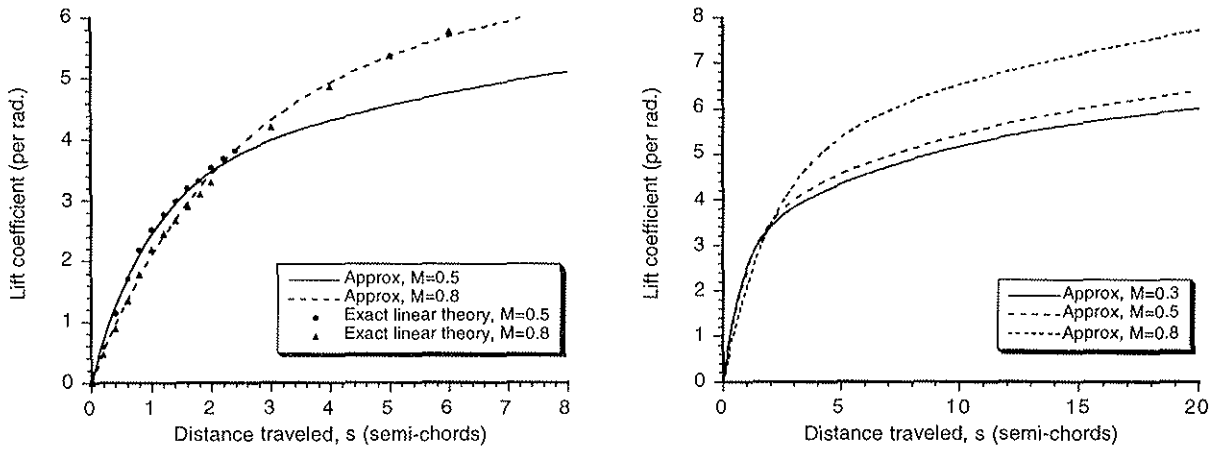


Figure 3: Indicial lift due to the penetration of a sharp-edge gust. Left figure: Comparison of exponential approximation with exact linear theory. Right figure: Exponential approximations at extended values of time

value ($\psi_g(\infty, M) = 1$) of the gust function. In addition, to obtain the best possible match to the exact linear theory, another constraint can be imposed by closely matching the exact time rate-of-change of lift at $s = 0$, again with the details being given in Ref. 47.

For $N = 1$, the errors were too large to render adequate approximations. For $N > 2$, approximately the same cost function resulted as for the $N = 2$ case. Because it is desirable to minimize the number of coefficients for numerical efficiency when using a superposition algorithm, the $N = 2$ case was selected. Results for the resulting sharp-edged gust functions are shown for Mach numbers of 0.5 and 0.8 in Fig. 3, with the coefficients being given in Table 1. It will be seen from Fig. 3 that the approximations match the exact solutions almost precisely at early values of time, as required. A summary of the gust responses for extended values of time is also shown in Fig. 3, where it is apparent that while the final values increase with increasing Mach number, the initial growth in lift is less as the Mach number increases. This can be im-

Gust Function	G_1	G_2	g_1	g_2
$\psi_g(s)$ (Ref. 36)	0.5	0.5	0.130	1.0
$\psi_g(s)$ (Ref. 27)	0.579	0.421	0.139	1.802
$\psi_g(s, M)$ (Linear)	0.527	0.473	0.100	1.367
$\psi_g(s, M)$ (CFD)	0.670	0.330	0.1753	1.637

Table 1: Summary of sharp-edged gust function coefficients

portant for transient problems such as BVI, where the effects of compressibility normally appear as increased lags in the development of the lift. In fact, this is exactly the opposite to that expected, either on the basis of quasi-steady assumptions or incompressible flow assumptions with a Glauert-type correction.

Determination of $\psi_g(s, M)$ from CFD

Results for 2-D flow were computed using TURNS (see Ref. 43) for a NACA 0012 encountering station-

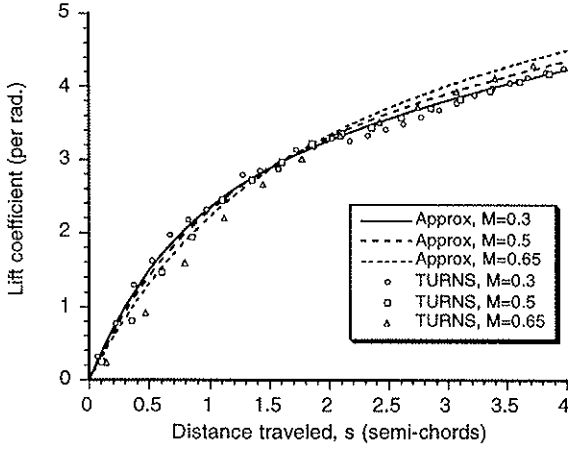


Figure 4: Comparisons of exponential sharp-edge gust function with results computed using TURNS at early values of time.

ary sharp-edge gusts at $M = 0.3, 0.5, 0.65$ and 0.8 . As mentioned previously, for the higher Mach number there was evidence of some non-linearity in the propagation of perturbations in the flow due to the development of a shock wave on the upper surface of the airfoil. For this case the data in the early stages was ignored; only data describing the asymptotic behavior for $s > 10$ were used. The time-scaling of the gust function by the factor β^2 as suggested previously appeared to be a feature confirmed by the CFD analysis, at least in the subsonic flow regime.

The resulting coefficients for this generalized sharp-edged gust function are also given in Table 1, and the results are plotted graphically in Fig. 4. The level of agreement of the exponential indicial approximation with the TURNS results is good, bearing in mind that this indicial function (Eq. 9) has constant coefficients and is generalized in terms of Mach number alone.

Response to an Arbitrary Gust

Within the assumptions of the linear theory a general stationary gust field $w_g(x, t)$ can be decomposed into a series of sharp-edged gusts of small magnitude. Using the indicial gust response the response to an arbitrary gust field can then be found using Duhamel superposition. For example, the response to a continuous gust field may be written analytically as

$$\Delta C_n^g(s) = \frac{2\pi}{\beta} \left[\frac{1}{V} \int_0^s \frac{dw_g}{d\sigma} \psi_g(s - \sigma, M) d\sigma \right] \quad (10)$$

where, as described previously, it is assumed that the in-plane variations in velocity produces only a quasi-steady effect. While the linearity of an arbitrary gust problem cannot necessarily be established a priori, especially for Mach numbers above the critical Mach number, the technique has been well proven using experimental measurements for unsteady airfoils in Refs. 25 and 26 and 46 for the Mach numbers typical of helicopter rotors, as well as for flap motion.^{27, 29}

Two numerical methods can be used to perform the superposition – the state-space form or recursive form. In discrete time a finite-difference approximation to

the Duhamel integral leads to a one-step recursive formulation, and the various numerical procedures have been developed in Ref. 46 and elsewhere for airfoil motion using the indicial function concept. These methods can also be easily applied to the gust problem. For example, denoting the current time step by t and the non-dimensional sample interval by Δs , the lift may be constructed from an accumulating series of small gust inputs using

$$\Delta C_{n_t}^g = \frac{2\pi}{\beta} \frac{1}{V} [\Delta w_g - Z_{1_t} - Z_{2_t}] = \frac{2\pi}{\beta} \alpha_{e_t} \quad (11)$$

Again, the $N = 2$ case for the gust function has been assumed. Note that α_e can be considered simply as a pseudo angle of attack, which represents the time-history of the unsteady aerodynamic effects. In this case, the deficiency functions, Z_{1_t} and Z_{2_t} , are analogous to aerodynamic states since they contain all the hereditary information about the aerodynamic forces. The deficiency functions are given by the one-step recursive formulas

$$\begin{aligned} Z_{1_t} &= Z_{1_{t-1}} E_1 + G_1 (\Delta w_{g_t} - \Delta w_{g_{t-1}}) \\ Z_{2_t} &= Z_{2_{t-1}} E_2 + G_2 (\Delta w_{g_t} - \Delta w_{g_{t-1}}) \end{aligned}$$

where $E_1 = \exp(-g_1 \beta^2 \Delta s)$ and $E_2 = \exp(-g_2 \beta^2 \Delta s)$, and where the subscripts t and $t-1$ are the current and previous time steps, respectively. The corresponding algorithms in state-space form for this superposition process are given in Ref. 47.

Acoustics Model

The acoustic pressure field can be calculated by using the acoustic analogy in the form of the Ffowcs Williams-Hawkins (FW-H) equation. In the present work Farassat's formulation-1 was used,⁴⁸ where the acoustic pressure can be written as

$$\begin{aligned} p'(x, y, z, \psi) &= \frac{1}{4\pi} \frac{\partial}{\partial t} \iint \left[\frac{\rho v_n}{\mathcal{R}(1 - M_{\mathcal{R}})} \right]_{\psi_{\tau}} dS \\ &+ \frac{1}{4\pi a} \frac{\partial}{\partial t} \iint \left[\frac{l_{\mathcal{R}}}{\mathcal{R}(1 - M_{\mathcal{R}})} \right]_{\psi_{\tau}} dS \\ &+ \frac{1}{4\pi} \frac{\partial}{\partial t} \iint \left[\frac{l_{\mathcal{R}}}{\mathcal{R}^2(1 - M_{\mathcal{R}})} \right]_{\psi_{\tau}} dS \quad (12) \end{aligned}$$

where $l_{\mathcal{R}}$ is the total force on the fluid at each source point on the blade in the direction of the observer, and ψ_{τ} is the retarded azimuthal time at that source point. The first term in Eq. 12 is the thickness noise; the second two terms are the loading noise, which are computed here using the indicial method. The quadrupole term has been neglected since for the cases considered in this paper the Mach numbers are mostly subcritical.

For the non-compact acoustic calculations presented in this paper, a chordwise pressure loading was synthesized for the loading (dipole) noise. Since the linearity assumptions of the indicial method do not allow for variations in the form of the chordwise pressure, an assumed pressure mode was used. In its simplest form this mode shape can be the (analytic) subsonic form or another (discretized) form as given by

the CFD analysis that is then linearly scaled as a function of angle of attack and the Glauert factor. For example, using linear theory the chordwise pressure can be written as

$$\Delta C_p(x, t) = \frac{4}{\beta} \sqrt{\frac{1-x}{x}} \alpha_e(t) \quad (13)$$

The thickness (monopole) noise was obtained from a source/sink thickness displacement model in a uniform free-stream flow, the free-stream flow being set equal the local blade sectional velocity, U_T . The simple thickness model given by Schmitz and Yu³ where

$$v_n(x) = U_T \frac{dy_t}{dx} \quad (14)$$

tends to provide a relatively crude model for the noise, and can affect the amplitude and waveform of the noise pulse at higher (subsonic) Mach numbers. A better result for the normal velocity perturbation (which is used here in the first term in Eq. 12) can be shown to be

$$v_n(x, y) = \frac{U_T}{\pi} \int_0^c \frac{dy_t}{dx'} \frac{y}{(x-x')^2 + y^2} dx' \quad (15)$$

where y_t is the airfoil thickness profile. This equation is solved numerically. In addition, for each chordwise source point the appropriate retarded azimuthal time must be computed – the fact that the pressure disturbances due to thickness do not arrive in-phase at the observer location leads to a negative sound pulse.

Note that the preference is normally to work with Farassat's formulation-1A of the FW-H, which is used in the WOPWOP code (see Ref. 49) and other codes. In this formulation the time-derivative must be evaluated over the blade surface since it appears inside the integral, and this tends to help suppress numerical noise. However, with formulation-1, the time derivative appears outside the surface integral and only a single numerical derivative over time needs to be evaluated. In the present approach with formulation-1, the acoustic pressure was evaluated at the correct retarded time using a discrete binning technique with linear weighting factors. The bin number was computed from the appropriate retarded azimuth (retarded time), with a typical bin size being one to one-half degrees of azimuth. For example, the azimuthal reception time ψ that a sound pressure signal generated at the source time ψ_τ is received at the observer location is given by

$$\psi = \left(\psi_\tau + \frac{\Omega \mathcal{R}}{a} \right) \frac{180}{\pi} \quad (16)$$

which is in units of degrees. The acoustic information is then sorted into the appropriate retarded azimuth bin, and weighted by applying linear weighting factors to adjacent bins.

One advantage of binning the acoustic information is computational efficiency since the results are fully available at the end of one rotor revolution; no post-processing with interpolation is required to compute the acoustics over the blade planform at the appropriate retarded time. However, with discrete binning one must ensure that the number of azimuthal source

time-steps where the airloads are computed is at least twice the number of discrete retarded time bins. If this requirement is not met, then some numerical noise will occur. Another advantage is that binning allows the rapid calculation of the acoustic planform. Binning has been found particularly attractive from the perspective of modeling active closed-loop control of the acoustics, for example with the use of trailing-edge flaps,²⁹ since it is necessary to provide a controller with information relating the time of pressure generation to the time of acoustic reception, i.e. the acoustic planform.

Results and Discussion

2-D BVI Problem

CFD calculations have been made using TURNS⁴⁵ to obtain the unsteady loads on a NACA 0012 airfoil interacting with a convecting vortex of non-dimensional strength $\hat{\Gamma} = 0.2$ traveling at a steady velocity 0.26 chords ($y_v = -0.26c$) below the airfoil. Typical helicopter advancing blade conditions at Mach numbers between 0.5 and 0.8 were considered, since these conditions serve to illustrate the influence of compressibility on the BVI problem. The CFD results were compared to solutions obtained using the indicial approach, which although restricted here to the calculation of the integrated airloads, has a relative computational speed advantage of about five orders of magnitude.

The tangential velocity in the interacting vortex was approximated using a Kaufmann/Scully vortex, namely

$$V_\theta(r) = \frac{\Gamma r}{2\pi(r_c^2 + r^2)} \quad (17)$$

where r is the distance along a radial line emanating from the center of the vortex such that $r^2 = (x - x_v)^2 + (y - y_v)^2$, and the vortex position x_v, y_v is relative to a coordinate axis at the leading-edge of the airfoil. A core size of $r_c = 0.05c$ was used, although the interaction between the airfoil and the vortex is sufficiently spaced in the cases considered that the core radius does not play a significant role. The reciprocal influence of the airfoil on the vortex convection velocity and trajectory was neglected.

Results for two subsonic Mach numbers and for a weakly transonic case are shown in Figs. 5 and 6, respectively. It can be seen in all cases that the influence of the vortex has affected the airfoil lift when it is well upstream of the airfoil leading-edge. This result is important for the computations because it sets a minimum upstream distance to establish the proper initial conditions for both the CFD and indicial approaches. Typically, a starting distance 10 chord lengths upstream is the minimum to avoid any sensitivity to initial conditions. A lift minimum was obtained just as the vortex reached the airfoil leading-edge ($x_v = 0$), followed by a rapid increase in the lift as the vortex passed downstream over the chord. The agreement between the indicial approach and the TURNS code is excellent at the subsonic Mach numbers, and these results essentially confirm the validity of linearity for BVI, at least under these conditions.

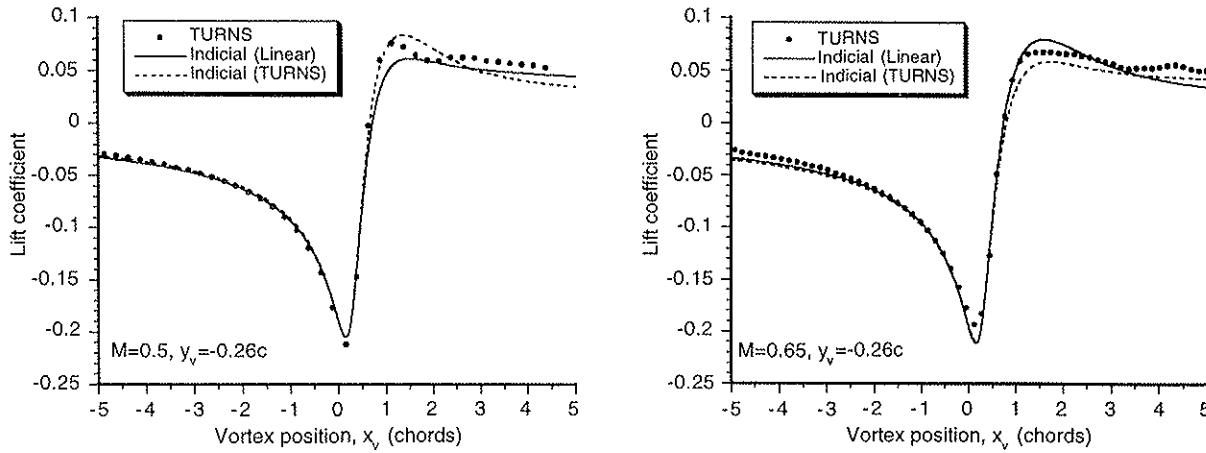


Figure 5: Comparison with TURNS result for a subsonic 2-D vortex-airfoil interaction, $\hat{\Gamma} = 0.2, y_0 = -0.26c, M = 0.5$ and $M = 0.65$

For the higher Mach number of 0.8, as shown in Fig. 6, the flow mildly exceeds the critical Mach number of this NACA 0012 section. However, the agreement in terms of peak-to-peak lift and phasing of the lift is still good, and much better than could possibly be obtained using the Küssner function, which will overpredict the peak-to-peak lift and the slope.⁴⁷ However, the results also show that with the indicial method there is a somewhat larger lift overshoot downstream of the airfoil trailing-edge compared to that predicted by TURNS. This is due to the supersonic pocket on the upper surface, which plays a role in delaying forward propagation of pressure disturbances from the adjustments taking place in the trailing-edge region. Such effects cannot be easily represented using the indicial method and, therefore, the occurrence of significant transonic flow defines an upper bound of applicability to the indicial method. However, as shown by Ballhaus,⁴² even for the transonic conditions linearity can hold so long as flow perturbations are small relative to the mean operating state.

It will also be seen from the results in Figs. 5 and 6 that the effects of increasing Mach number serves to attenuate the peak-to-peak value of the lift response, which is exactly opposite to that given by incompressible unsteady theory even with a Glauert correction. Furthermore, it is apparent that the effects of increasing Mach number introduces a larger phase lag in the lift response (the slope is less during the interaction), and this obviously becomes a significant consideration for accurate noise predictions since these depend on the time rate-of-change of the airfoil surface pressures.

3-D BVI Problem

The 3-D BVI problem is considerably more complicated than for the 2-D case discussed above. Besides the fact that now both trailed as well as shed vorticity appears in the wake of the blade, the elements of the rotating blades travel at different velocities relative to the vortex field so the unsteady flow adjustments on the blades take place over different time scales when viewed in terms of rotor time (ψ). Obviously for an actual helicopter, when multiple blades and their as-

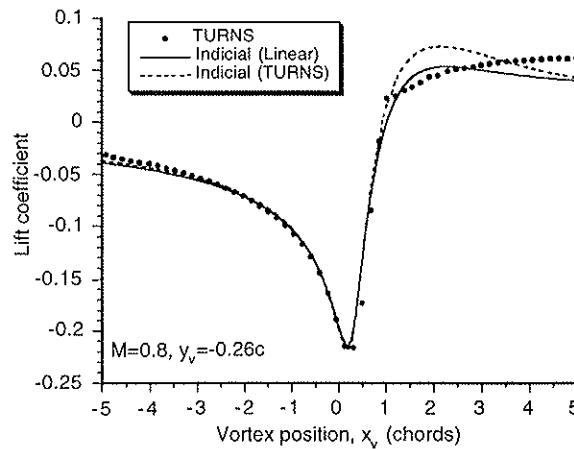


Figure 6: Comparison with TURNS result for a mildly transonic 2-D vortex-airfoil interaction, $\hat{\Gamma} = 0.2, y_0 = -0.26c, M = 0.8$

sociated tip vortices are involved, identifying individual BVI events and their associated time-scales to the point of validating an aerodynamic model is basically impossible. Here, besides the unsteady aerodynamic model, a key element in the problem is predicting the tip vortex strengths and locations relative to the rotor blades. This is a problem unto itself that has not yet been completely resolved.

To eliminate the uncertainties associated with the rotor wake, several simpler BVI experiments with rotors have been conducted in the controlled environment of wind-tunnels. These experiments include the work of Surendraiah,⁵⁰ Caradonna *et al.*,⁵¹ Kokkalis *et al.*⁵² and Seath *et al.*⁵³ These experiments are based on rigid non-articulated one or two-bladed rotors that encounter an isolated line vortex generated upstream of the rotor. The rotors are operated at nominally zero thrust, thereby minimizing the self-generated wake and allowing the effects of the generator vortex on the blade airloads and acoustics to be studied, essentially in isolation.

Although the above cited works have concentrated on similar problems, the recent work of Kitaplioglu and Caradonna^{54, 55} is probably more useful for validating the BVI aeroacoustics problem because both unsteady blade loads and acoustic pressures were measured simultaneously. The results for eight combinations of vortex sign and vortex location relative to the rotor have been documented, although only a subset of these cases will be discussed in the present paper.

In the Kitaplioglu and Caradonna experiment, a two-bladed rigid rotor encountered a vortex (generated by a wing placed about three rotor radii upstream of the rotor shaft) of measured strength and location relative to the rotor. The BVI event took place over the upstream edge of the rotor disk, where the blade was effectively parallel to the longitudinal axis of the generator vortex. While BVI may be expected on the downstream blade as well, the effects of the hub were known to diffuse the vortex and no significant BVI was apparent in the measured airloads near $\psi = 0$. The location of the generating vortex relative to the rotor (blade) was changed by adjusting the position of a generating wing, with the vortex sign and strength being changed by altering the wing angle of attack. For the present work, a non-dimensional generator vortex strength of $\hat{\Gamma} = \Gamma / (V_\infty c_{ref}) = 0.36$ was used with a viscous core size that was 5% of the generating wing chord, c_{ref} , these parameters being based on the measurements of Takahashi and McAlister.⁵⁶ In addition, the tangential (swirl) velocity of the vortex has been found to closely correspond to Eq. 17.

Unsteady Airloads

The unsteady airloads on the rotor were modeled by applying the indicial method at 30 radial stations along the blade. Induced effects from the near trailed wake were modeled by means of a Wessinger L-type method. In this approach the three-dimensional spanwise loading (therefore including both trailed and shed wake effects) is computed by an influence function method, requiring the solution of a set of coupled linear simultaneous equations at each time step. The indicial functions are integrated into the right-hand-side of these equations. This approach is typical of that used in comprehensive rotor codes. The unsteady airloads were measured with 60 pressure transducers that were distributed over three spanwise stations at 77%, 88% and 95% of blade radius. Since the indicial approach requires integrated airloads, the chordwise pressures measured at the three radial blade locations were numerically integrated.⁴⁷

The time-histories of the unsteady normal force coefficient at the three radial stations on the reference blade are shown in Fig. 7, and the corresponding spanwise loading is shown in Fig. 8 for the case where the generator vortex has a negative strength and with the vortex passing 0.25 chords below the blade. Results are shown with the indicial method and by using TURNS directly. While the overall agreement of the predictions with experimental airloads data was found to be good, with the indicial method there was a tendency to over-predict the peak-to-peak amplitude of the unsteady airloads. The TURNS code gives uniformly excellent predictions, although this is at the expense of about five orders of magnitude in terms of

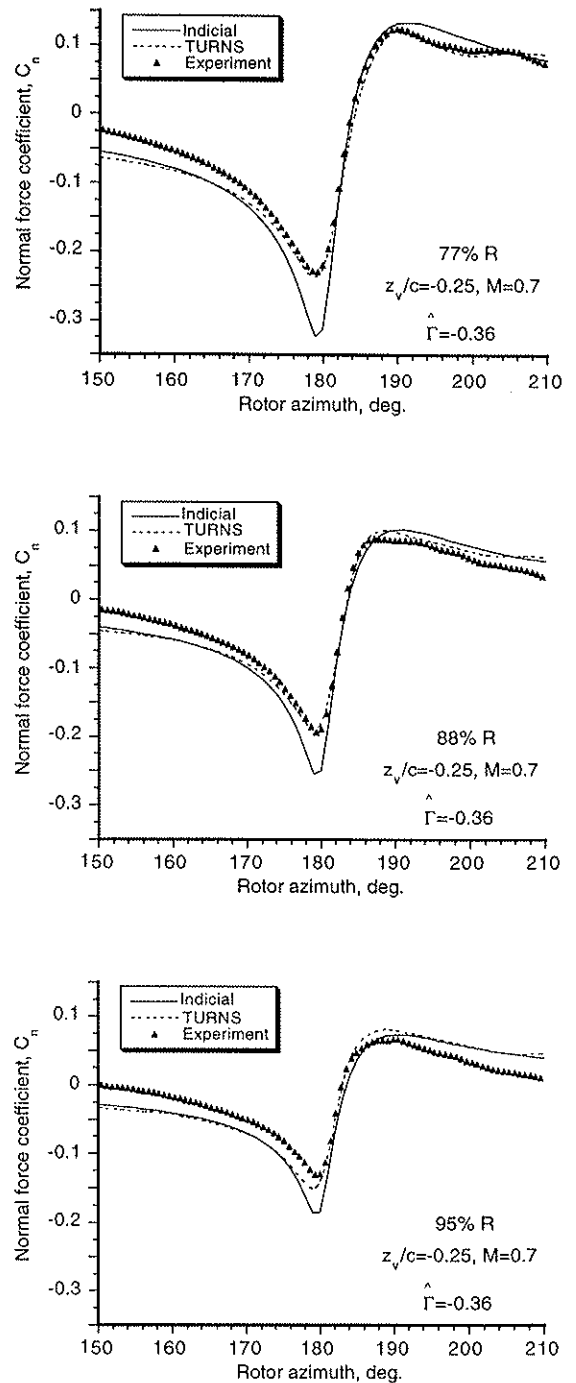


Figure 7: Comparison of indicial results during a 3-D BVI with experimental measurements of sectional normal force at three spanwise stations, $M_{tip} = 0.7$, $z_v = -0.25$

computational cost.

Like the 2-D case, the airloads varied rapidly with respect to rotor azimuth position, changing sign as the blade passed from one side of the vortex to the other. Although the BVI event in this case is nominally parallel, successive parts of the blade encounter the vortex over a finite range of azimuth angles with the interaction effectively sweeping from the root of

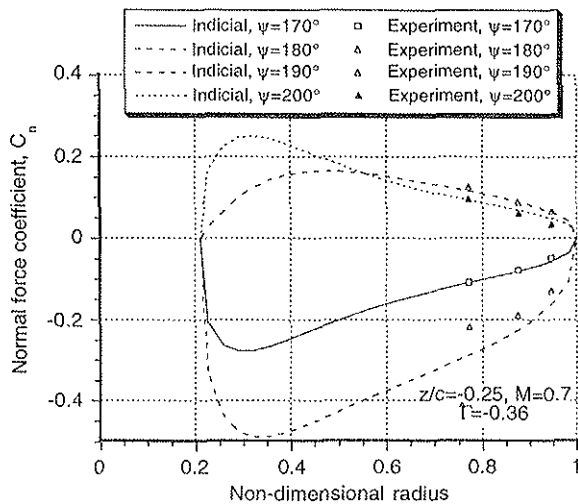


Figure 8: Spanwise distribution of C_n just before and just after the BVI, $M_{tip} = 0.7$, $z_v = -0.25$

the blade out toward the tip. Under these conditions some three-dimensionality is produced, and this can be seen in the spanwise loading of Fig. 8 just after the BVI at $\psi = 180^\circ$. Since the blade is untwisted the C_n distribution is nominally hyperbolic, but because the flow adjustments take place over a finite number of chord lengths of airfoil travel, the adjustments inboard take place over a greater change in ψ . Recall that it is the slope of the C_n curve or the time rate-of-change of the airloads during the interaction that is important from the perspective of the acoustics. Incompressible unsteady theory will always over-predict this slope, therefore, it will also over-predict the magnitude of the acoustic pulse.

Acoustics

As described in Refs. 54 and 55, the acoustics were measured by arrays of microphones located both in the near-field (roughly 0.5 of rotor radius away) and the far-field (roughly 3 rotor radii away) relative to the rotational axis, with both microphone sets on the retreating side of the rotor. In general, both the near-field and far-field acoustics are sensitive to the phasing of the unsteady airloads during the BVI. In addition, the duration and phasing of the BVI event along the blade, the Doppler magnification, and the distance of the event to the microphone location combine to produce the net sound pressure signature at a given time. The thickness sound pressure further combines with the loading term, resulting in small variations in phasing that can significantly affect the net noise signature.

The effects of the thickness and loading terms can be better understood by computing the instantaneous acoustic field, examples of which are shown in Figs. 9 and 10. These results were computed for 2 rotor radii below the rotor plane ($z/R = -2.0$) on a 161-by-161 grid of $\pm 8R$. In this case the generator vortex was 0.25 chords below the rotor plane and with a negative circulation. Note from these figures the proliferation of acoustic waves generated by the rotor. The thickness

noise, which is shown in the left of Fig. 9, consists of crescent shaped wave fronts that spiral away from the rotor tips along the characteristic curves. The loading noise due to the BVI event is shown in the right of Fig. 9. The BVI occurs over the front of the rotor; at the rear of the rotor the generator vortex is diffused and no significant BVI occurs. Therefore, in the modeling the vortex was assumed to terminate at the hub. Acoustically the single BVI event produces an almost spherical wave front that propagates at the speed of sound, and appears in Fig. 9 as a growing circular ring as the wave front intersects the measurement plane.

Figure 10 shows the net acoustic contours, where the thickness and loading terms are combined. Since the respective wave fronts have different intensities and different orientations to each other, the combined effect on the acoustic field is quite complicated. Note that the spiral (thickness noise) and circular (BVI loading noise) wave fronts combine in some locations of the acoustic field but reinforce in other regions, thereby leading to a strong directivity pattern. Calculations of the acoustic contours for this problem are also given by Strawn *et al.*¹⁰ using CFD coupled with the Kirchhoff method.

The acoustic directivity pattern can be examined using the sound pressure level (SPL). Results are shown in Figs. 11 for an $x-z$ plane 3 rotor radii away on the retreating side of the rotor and also on a $x-y$ plane 3 radii below the rotor. The thickness noise is focused in the rotor plane and is most intense when the blade tip is advancing toward the observer. This is due to the Doppler factor that appears in all three terms in the FW-H equation. The thickness SPL is distributed symmetrically above and below the rotor, and drops off quickly in intensity when moving out of the rotor plane. Accordingly, there is little thickness noise below the rotor except in the far-field, but this is of very low intensity since it drops off like $1/R$.

Unlike the thickness noise, the BVI loading noise is distributed anti-symmetrically with the sign changing depending on whether the observer location is below or above the rotor plane. With a negative vortex strength, which generates the airloads shown previously in Fig. 7, there is a positive sound pulse produced above the rotor and a negative pulse below. The net effect of these SPL directivity patterns is shown in Fig. 11, such that when the thickness and BVI loading noise sources are combined the terms reinforce above the rotor whereas below the rotor they partially cancel. The result in this case is well focused sound pressure levels above the rotor plane. Of course, the result is reversed by changing the sign of the generator vortex whereby the noise will become focused below the rotor plane.

Further details of the sound field can be understood from the time-histories at specific points. Sample predictions of the time-histories of the near-field sound pressure are shown in Fig. 12 and are compared with acoustic pressures computed using the TURNS code.⁵⁷ In the first case, the indicial method gives excellent agreement with the test data whereas TURNS overpredicts the peak-to-peak pressure. However, TURNS produces a better correlation with the test data at the trailing-edge of the pulse. This is expected due to the more complicated nature of the flow physics on the blade in this region, which involves

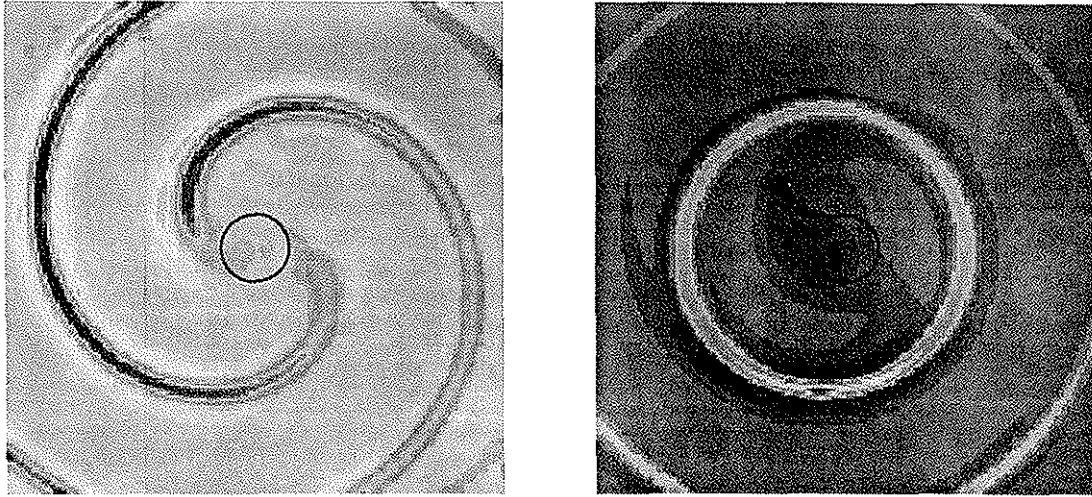


Figure 9: Acoustic waves produced by the rotor at $\psi_b = 30^\circ$, $M_{tip} = 0.7$, $z_v = -0.25$. Left: Thickness noise. Right: Loading (BVI) noise. 161 by 161 grid, $\pm 8R$ from rotor.

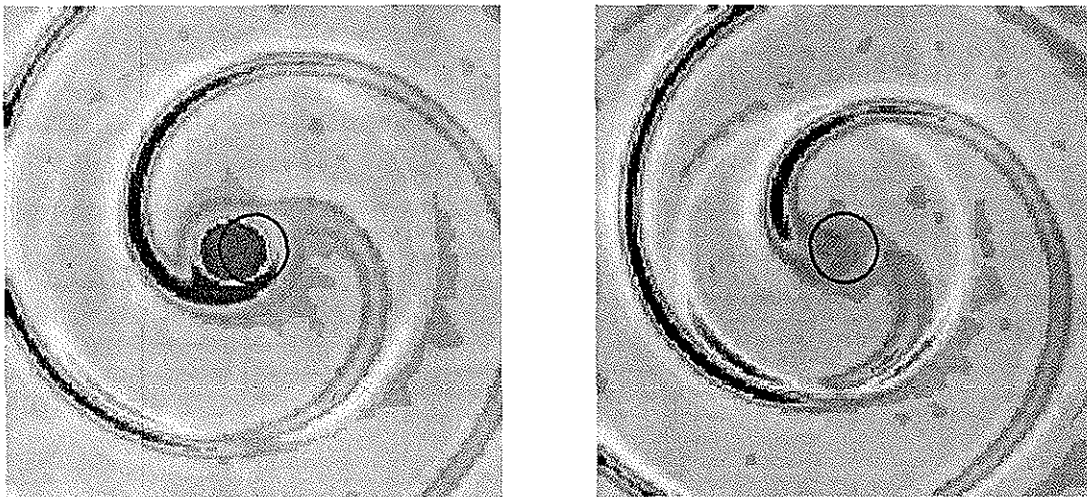


Figure 10: Acoustic waves produced by the rotor, including both thickness and loading noise, $M_{tip} = 0.7$, $z_v = -0.25$. Left: Just after BVI event. Right: Later time showing propagation of BVI wave front. 161 by 161 grid, $\pm 8R$ from rotor.

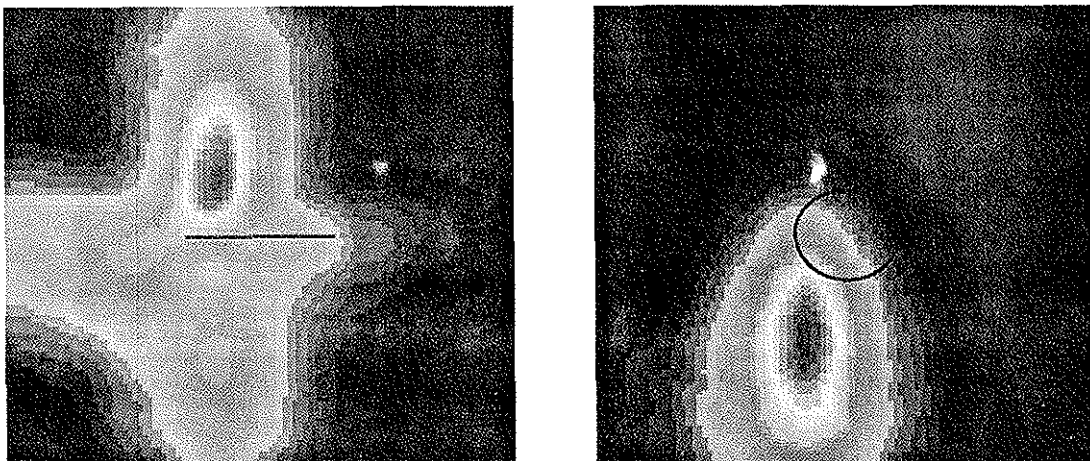


Figure 11: SPL directivity patterns from rotor, $M_{tip} = 0.7$, $z_v = -0.25$. Left: $y = -3R$, $x - z$ plane, retreating side of rotor. Right: $z = -3R$, $x - y$ plane, below rotor. $\pm 5R$ from rotor.

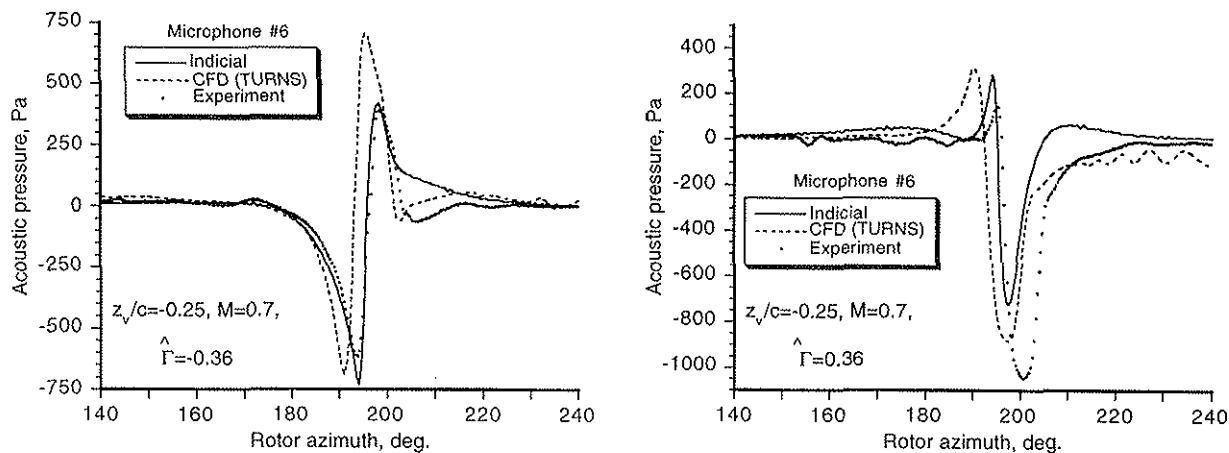


Figure 12: Comparison of near-field acoustic pressures at microphone 6 using indicial method and TURNS, $z/c = -0.25$. Left: $\hat{\Gamma} = -0.36$. Right: $\hat{\Gamma} = 0.36$

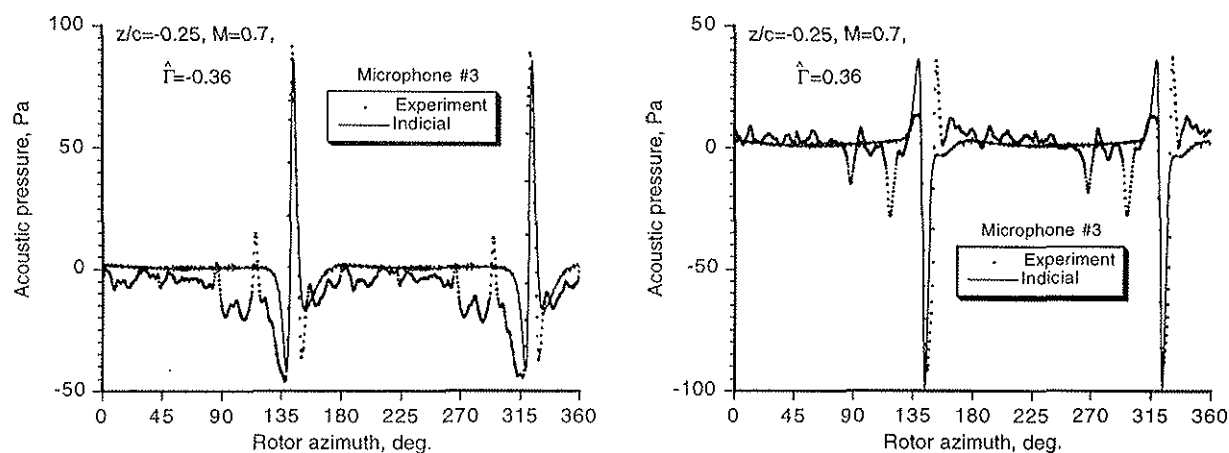


Figure 13: Far-field acoustic pressures at microphone 3, $z/c = -0.25$. Left: $\hat{\Gamma} = -0.36$. Right: $\hat{\Gamma} = 0.36$

the three-dimensional upstream propagation of pressure disturbances from the trailing-edge and tips of the blade. This effect is not explicitly represented in the indicial method. The slight phase shift in the CFD results is due to a 0.11 chord lateral offset in the assumed location of the generator vortex, a fact that only became apparent after the CFD calculations had been performed. Note that the acoustic pulse is received at the near-field microphone locations only about 10 degrees after the BVI event. In the second case, with the opposite sign on the generator vortex, both methods underpredict the minimum pressure but the pulse shape is essentially correct in both cases. Again, as expected, TURNS give a better agreement at the trailing-edge of the pulse.

The far-field acoustics are considerably less in overall intensity, the peak sound pressures being about 20 dB lower than in the near-field. Referring to Fig. 13, note that the time-histories of the acoustic pressures take on the characteristic positive or negative going pulse (depending on the sign of the generator vortex) that has become well known as typical of BVI.^{1, 2} There are two acoustic pulses per rotor revolution because each blade interacts with the generator vortex 180-degrees apart. Because of the lower

intensity sound pressures, the far-field sound pressures levels exhibit more “noise,” in part, due to reflections from the wind-tunnel walls. It will be seen that in the far-field the pressure pulse is received some 140 degrees of blade rotation after the BVI event. Only a mild directivity existed for the four microphones in the far-field, so the magnitude and pulse shape of the sound pressure was much the same for all of the microphones. Figure 13 indicates that the current predictions are in good agreement with the measured values.

Conclusions

An approach has been described to calculate the aeroacoustics of BVI using the indicial method. Comparisons with CFD results for model 2-D problems show that the unsteady lift on an airfoil during encounters with vortices in subsonic flow can be computed accurately using indicial methods. From the results given in this paper it has been shown that both the magnitude and phasing of the unsteady airloads are sensitive to compressibility effects during a BVI encounter. One advantage of the indicial method is computational efficiency being approximately four to five orders of magnitude faster than a CFD based anal-

ysis. Another advantage is that the airloads can be written in a numerical form that lends to implementation inside a comprehensive rotor analysis, and also potentially to active acoustic control formulations.

When integrated into a 3-D rotor simulation with the use of the acoustic analogy in the form of the FW-H equation, the indicial method has provided good agreement with unsteady airloads measured on the blades during a BVI event. Both the near and far-field acoustic pressures were found to be predicted with good accuracy. In all cases, the essential character of the acoustic signature was well represented. Along with the attractive computational benefits, such levels of correlation obtained give considerable credibility to the indicial approach for aeroacoustic studies, and is currently forming the framework for ongoing work in the area of active acoustic control.

Acknowledgments

The author thanks Vasudev Parameswaran, Megan McCluer and James Baeder for providing the CFD results. Thanks also to Francis Caradonna and Cahit Kitaplioglu of NASA Ames for providing the airloads and acoustics data from their BVI experiment.

References

- ¹Schmitz, F. H., "Rotor Noise," Chapter 2, *Aeroacoustics of Flight Vehicles: Theory and Practice*, Vol. 1, NASA Reference Publication, 1258, Aug. 1991.
- ²Schmitz, F. H. and Yu, Y. H., "Helicopter Impulsive Noise: Theoretical and Computational Status," *Journal of Sound and Vibration*, Vol. 109, No. 3, 1986, pp. 361-421.
- ³Schmitz, F. H. and Yu, Y. H., "Theoretical Modeling of High Speed Helicopter Impulsive Noise," Paper 54, 3rd European Rotorcraft Forum, Aix-en-Provence, France, Sept. 7-9, 1977.
- ⁴Widnall, S., "Helicopter Noise due to Blade-Vortex Interaction," *Journal for the Acoustical Society of America*, Vol. 50, No. 1 (Pt. 2), 1971.
- ⁵Nakamura, Y., "Prediction of Blade-Vortex Interaction Noise from Measured Blade Pressure Distributions," Paper No. 32, Proceedings of the 7th. European Rotorcraft Forum, September 1981.
- ⁶McCroskey, W. J. and Goorjian, P. M., "Interactions of Airfoils with Gusts and Concentrated Vortices in Unsteady Transonic Flow," AIAA Paper 83-1691, July 1983.
- ⁷Srinivasan, G. R. and McCroskey, W. J., "Numerical Simulations of Unsteady Airfoil Interactions," *Vertica* Vol. 11, No. 1/2, 1987, pp. 3-28.
- ⁸Baeder, J. D., "Computation of Non-Linear Acoustics in Two-Dimensional Blade-Vortex Interactions," Paper 1-1, Proceedings of the 13th European Rotorcraft Forum, Sept. 1987.
- ⁹Lyrantzis, A. S., "Review: The Use of Kirchhoff's Method in Computational Acoustics," *Journal of Fluids Engineering*, Vol. 116, Dec. 1994, pp. 665-675.
- ¹⁰Strawn, R. C., "New Computational Methods for the Prediction and Analysis of Helicopter Noise," AIAA Paper 96-1696, 2nd AIAA/CEAS Aeroacoustics Conference, State College, PA, May 6-8, 1996.
- ¹¹Dawson, S., "Wind Tunnel Test of an Active Flap Rotor: BVI Noise and Vibration Reduction," Proceedings of the American Helicopter Society, 51st Annual Forum, Fort Worth, Texas, May 9-11, 1995.
- ¹²Milgram, J. and Chopra, I., "Helicopter Vibration Reduction with Trailing Edge Flaps," American Helicopter Society Aeromechanics Specialists Meeting, Fairfield, CT, Oct. 11-13, 1995.
- ¹³Ben-Zeev, O. and Chopra, I., "Advances in the Development of an Intelligent Helicopter Rotor Employing Smart Trailing-Edge Flaps," *Smart Materials and Structures*, Vol. 5, 1996, pp. 11-15.
- ¹⁴Tung, C., Gallman, J. M., Kube, R., Wagner, W., van der Wall, B., Brooks, T. F., Burley, C. L., Boyd, D. D., Rahier, G., and Beaumier, P., "Prediction and Measurement of Blade Vortex-Interaction Loading," Proceedings of the 1st Joint CEAS/AIAA Aeroacoustics Conference, Munich, Germany, June 12-15, 1996.
- ¹⁵Lomax, H., "Indicial Aerodynamics," Chapter 6, *AGARD Manual on Aeroelasticity*, Oct. 1968.
- ¹⁶Tobak, M. and Schiff, L. B., "Aerodynamic Mathematical Modeling - Basic Concepts," *Dynamic Stability Parameters*, AGARD LS-114, 1981.
- ¹⁷Sears, W. R., "Some Aspects of Non-Stationary Airfoil Theory and Its Practical Application," *Journal of the Aeronautical Sciences*, Vol. 8, No. 3, Jan. 1941, pp. 104-108.
- ¹⁸Küssner, H. G., "General Airfoil Theory," NASA TM 979, 1941.
- ¹⁹von Karman, T. and Sears, W. R., "Airfoil Theory for Non-Uniform Motion," *Journal of the Aeronautical Sciences*, Vol. 5, No. 10, Aug. 1938, pp. 379-390.
- ²⁰Lomax, H., Heaslet, M. A., Fuller, F. B. and Sluder, L., "Two and Three Dimensional Unsteady Lift Problems in High Speed Flight," NACA Report 1077, 1952.
- ²¹Heaslet, M. A. and Sprieter, J. R., "Reciprocity Relations in Aerodynamics," NACA Report 1119, Feb. 1952.
- ²²Mazelsky, B., "Determination of Indicial Lift and Moment of a Two-Dimensional Pitching Airfoil at Subsonic Mach Numbers from Oscillatory Coefficients with Numerical Calculations for a Mach Number of 0.7," NACA TN 2613, Feb. 1952.
- ²³Mazelsky, B. and Drischler, J. A., "Numerical Determination of Indicial Lift and Moment Functions of a Two-Dimensional Sinking and Pitching Airfoil at Mach Numbers 0.5 and 0.6," NACA TN 2739, 1952.
- ²⁴Leishman, J. G., "Indicial Lift Approximations for Two-Dimensional Subsonic Flow as Obtained from Oscillatory Measurements," *Journal of Aircraft*, Vol. 30, No. 3, May/June 1993, pp. 340-351.
- ²⁵Leishman, J. G., "Modeling of Subsonic Unsteady Aerodynamics for Rotary Wing Applications," *Journal of the American Helicopter Society*, Vol. 35, No. 1, Jan. 1990, pp. 29-38.

- ²⁶Leishman, J. G. and Nguyen, K. Q., "State-Space Representation of Unsteady Airfoil Behavior," *AIAA Journal*, Vol. 28, No. 5, May 1990, pp. 836-844.
- ²⁷Leishman, J. G. "Unsteady Lift of an Airfoil with a Trailing-Edge Flap Based on Indicial Concepts," 18th European Rotorcraft Forum, Avignon, France, Sept. 15-18, 1992.
- ²⁸Leishman, J. G., "Unsteady Lift of an Airfoil with a Trailing-Edge Flap based on Indicial Concepts," *Journal of Aircraft*, Vol. 31, No. 2, March-April, 1994.
- ²⁹Hariharan, N., "Unsteady Aerodynamics of a Flapped Airfoil in Subsonic Flow Using Indicial Concepts," MS Thesis, University of Maryland, 1995.
- ³⁰Leishman, J. G. and Beddoes, T. S., "A Semi-Empirical Model for Dynamic Stall," *Journal of the American Helicopter Society*, Vol. 34, No. 3, July 1989, pp. 3-17.
- ³¹Tyler, J. C. and Leishman, J. G., "An Analysis of Pitch and Plunge Effects on Unsteady Airfoil Behavior," *Journal of the American Helicopter Society*, Vol. 37, No. 3, July 1992, pp. 69-82.
- ³²Leishman, J. G. and Crouse, G. L., Jr., "A State-Space Model for Unsteady Airfoil Behavior and Dynamic Stall," AIAA paper 89-1319, Proceedings of the AIAA/AHS/ASME Structural Dynamics and Materials Conference, Mobile, Alabama, April 1989.
- ³³Leishman, J. G., "Modeling of Sweep Effects on Dynamic Stall," *Journal of the American Helicopter Society*, Vol. 34, No. 3, July 1989, pp. 18-29.
- ³⁴Horlock, J. H., "Fluctuating Lift Forces on Airfoils Moving Through Transverse and Chordwise Gusts," *Journal of Basic Engineering*, Dec. 1968, pp. 494-500.
- ³⁵Miles, J. W., "The Aerodynamic Force on an Airfoil in a Moving Gust," *Journal of the Aeronautical Sciences*, Vol. 23, Nov. 1956.
- ³⁶Bisplinghoff, R. L., Ashley H. and Halfman, R. L., *Aeroelasticity*, Addison-Wesley Publishing Co., Reading, Mass., 1955.
- ³⁷van der Wall, B. and Leishman, J. G., "The Influence of Variable Flow Velocity on Unsteady Airfoil Behavior," *Journal of the American Helicopter Society*, Vol. 39, No. 4, October 1994, pp. 288-297.
- ³⁸Goldstein, M. E., *Aeroacoustics*, NASA SP-346, 1974.
- ³⁹Lomax, H., "Lift Developed on Unrestrained Rectangular Wings Entering Gusts at Subsonic and Supersonic Speeds," NACA Technical Note 2925, April 1953.
- ⁴⁰Garrick, I. E., "On Some Fourier Transforms in the Theory of Nonstationary Flows," Proceedings for the Fifth International Congress for Applied Mechanics, pp. 590-593, New York, 1939.
- ⁴¹Stahara, S. S. and Spreiter, J. R., "Research on Unsteady Transonic Flow Theory," Neilson Engineering and Research Report, NEAR TR-107, Jan. 1976.
- ⁴²Ballhaus, W. F. and Goorjian, P. M., "Computation of Unsteady Transonic Flows by the Indicial Method," *AIAA Journal*, Vol. 16, No. 2, Feb. 1978, pp. 117-124.
- ⁴³Parameswaran, V., "Concepts for the Reduction of Blade Vortex Interaction Noise and the Use of CFD to Determine Indicial and Gust Responses of an Airfoil in Compressible Flow," University of Maryland, Dept. of Aerospace Engineering, August 1995.
- ⁴⁴Singh, R. and Baeder, J. D., "The Direct Calculation of Indicial Lift Response of a Wing Using Computational Fluid Dynamics," AIAA 96-2508, 14th AIAA Applied Aerodynamics Conference, New Orleans, LA, June 17-20, 1996.
- ⁴⁵Srinivasan, G. R., Baeder, J. D., Obayashi, S. and McCroskey, W. J., "Flowfield of a Lifting Rotor in Hover: A Navier-Stokes Simulation," *AIAA Journal*, Vol. 30, No. 10, Oct. 1992, pp. 2371-2378.
- ⁴⁶Beddoes, T. S., "Practical Computation of Unsteady Lift," *Vertica* Vol. 8 No. 1, 1984, pp. 55-71.
- ⁴⁷Leishman, J. G., "Aerocoustics of 2-D and 3-D Blade Vortex Interaction Using the Indicial Method," American Helicopter Society 52nd Annual Forum, Washington DC, June 4-6, 1996.
- ⁴⁸Farassat, F., "Linear Acoustic Formulas for Calculation of Rotating Blade Noise," *AIAA Journal*, Vol. 19, No. 9, Sept. 1981, pp. 1122-1130.
- ⁴⁹Brentner, K. S., "Prediction of Helicopter Rotor Discrete Frequency Noise," NASA Technical Memorandum 87721, Oct. 1986.
- ⁵⁰Surendraiah, M., "An Experimental Study of Rotor Blade-Vortex Interaction," NASA CR-1573, May 1970.
- ⁵¹Caradonna, F. X., Laub, G. H. and Tung, C., "An Experimental Investigation of the Parallel Blade-Vortex Interaction," Workshop on Blade Vortex Interaction, NASA Ames Research Center, Oct. 1984.
- ⁵²Kokkalis, T. and Galbraith, R. A., "Description of, and Preliminary Results from a New Blade-Vortex Interaction Test Facility," Paper 80, 12th European Rotorcraft Forum, Garmish, Germany, Sept. 1986.
- ⁵³Seath, D. D., Kim, J.M. and Wilson, D. R., "An Investigation of the Parallel Blade-Vortex Interaction in a Low Speed Wind-Tunnel," AIAA Paper 87-1344, 19th Fluid Dynamics, Plasma Dynamics and Lasers Conference, Honolulu, June 8-10, 1987.
- ⁵⁴Kitaplioglu, C. and Caradonna, F. X., "Aerodynamics and Acoustics of Blade Vortex Interaction Using an Independently Generated Vortex," American Helicopter Society Aeromechanics Specialists Conference, San Francisco, CA, Jan. 19-21, 1994.
- ⁵⁵Kitaplioglu, C., Caradonna, F. X. and Burley, C. L., "Parallel Blade-Vortex Interactions: An Experimental Study and Comparison with Computation," American Helicopter Society Aeromechanics Specialists Conference, Bridgeport, CT, Oct. 11-13, 1995.
- ⁵⁶Takahashi, R. K. and McAlister, K. W., "Preliminary Study of a Wing-Tip Vortex Using Laser Velocimetry," NASA TM 88343, Jan. 1987.
- ⁵⁷McCluer, M. S. and Baeder, J. D., "Comparison of Experimental Blade-Vortex Interaction Noise with Computational Fluid Dynamic Calculations," American Helicopter Society 51st Annual Forum, Fort Worth, TX, May 9-11, 1995.